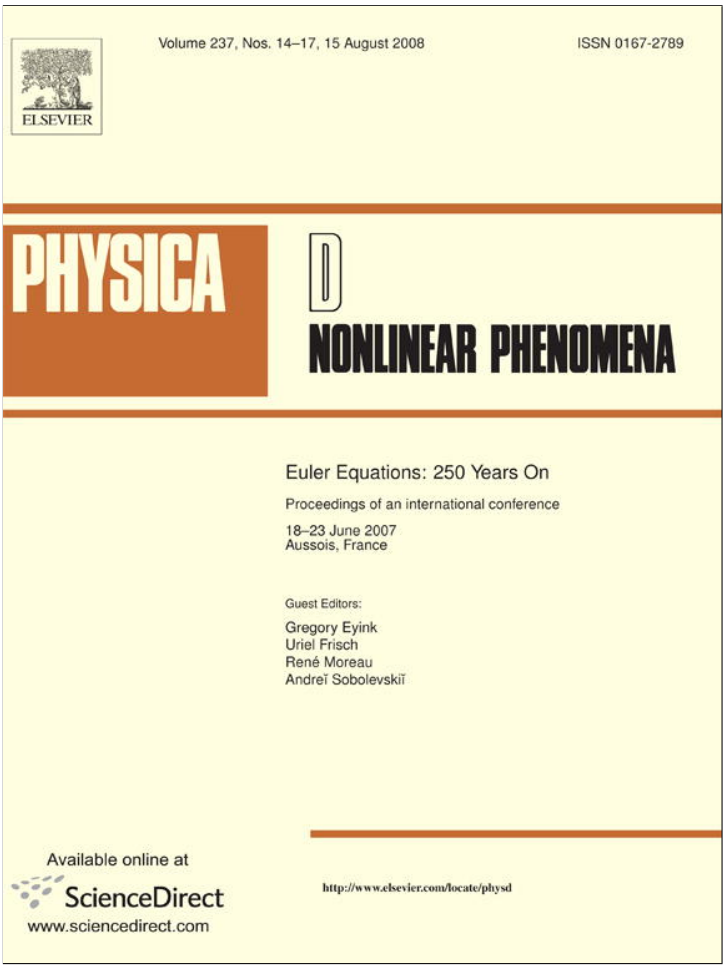

Available online at www.sciencedirect.com
ScienceDirect
Physica D 237 (2008) 2111–2126
PHYSICA D
www.elsevier.com/locate/physd

Climate dynamics and fluid mechanics: Natural variability and related uncertainties

Michael Ghil[a,b,c,d,*], Mickaël D. Chekroun[d], Eric Simonnet[e]

[a] *Département Terre-Atmosphère-Océan and Laboratoire de Météorologie Dynamique (CNRS and IPSL), École Normale Supérieure, 75231 Paris Cedex 05, France*
[b] *Department of Atmospheric Sciences, University of California, Los Angeles, CA 90095-1565, USA*
[c] *Institute of Geophysics and Planetary Physics, University of California, Los Angeles, CA 90095-1565, USA*
[d] *Environmental Research and Teaching Institute, École Normale Supérieure, 75231 Paris Cedex 05, France*
[e] *Institut Non Linéaire de Nice (INLN)-UNSA, UMR 6618 CNRS, 1361, route des Lucioles 06560 Valbonne, France*

Available online 1 April 2008

Abstract

The purpose of this review-and-research paper is twofold: (i) to review the role played in climate dynamics by fluid-dynamical models; and (ii) to contribute to the understanding and reduction of the uncertainties in future climate-change projections. To illustrate the first point, we review recent theoretical advances in studying the wind-driven circulation of the oceans. In doing so, we concentrate on the large-scale, wind-driven flow of the mid-latitude oceans, which is dominated by the presence of a larger, anticyclonic and a smaller, cyclonic gyre. The two gyres share the eastward extension of western boundary currents, such as the Gulf Stream or Kuroshio, and are induced by the shear in the winds that cross the respective ocean basins. The boundary currents and eastward jets carry substantial amounts of heat and momentum, and thus contribute in a crucial way to Earth's climate, and to changes therein.

Changes in this double-gyre circulation occur from year to year and decade to decade. We study this low-frequency variability of the wind-driven, double-gyre circulation in mid-latitude ocean basins, via the bifurcation sequence that leads from steady states through periodic solutions and on to the chaotic, irregular flows documented in the observations. This sequence involves local, pitchfork and Hopf bifurcations, as well as global, homoclinic ones.

The natural climate variability induced by the low-frequency variability of the ocean circulation is but one of the causes of uncertainties in climate projections. The range of these uncertainties has barely decreased, or even increased, over the last three decades. Another major cause of such uncertainties could reside in the structural instability – in the classical, topological sense – of the equations governing climate dynamics, including but not restricted to those of atmospheric and ocean dynamics.

We propose a novel approach to understand, and possibly reduce, these uncertainties, based on the concepts and methods of random dynamical systems theory. The idea is to compare the climate simulations of distinct general circulation models (GCMs) used in climate projections, by applying stochastic-conjugacy methods and thus perform a stochastic classification of GCM families. This approach is particularly appropriate given recent interest in stochastic parametrization of subgrid-scale processes in GCMs.

As a very first step in this direction, we study the behavior of the Arnol'd family of circle maps in the presence of noise. The maps' fine-grained resonant landscape is smoothed by the noise, thus permitting their coarse-grained classification.

Keywords: Climate change; Physical oceanography; Dynamical systems; Bifurcations; Structural stochastic stability; Arnol'd tongues

1. Introduction

Charney et al. [1] were the first to attempt a consensus estimate of the equilibrium sensitivity of climate to changes in atmospheric CO_2 concentrations. The result was the now famous range for an increase of 1.5–4.5 K in global near-surface air temperatures, given a doubling of CO_2 concentration.

As the relatively new science of climate dynamics evolved through the 1980s and 1990s, it became quite clear – from observational data, both instrumental and paleoclimatic, as well as model studies – that Earth's climate never was and is

* Corresponding author at: Département Terre-Atmosphère-Océan and Laboratoire de Météorologie Dynamique (CNRS and IPSL), École Normale Supérieure, 75231 Paris Cedex 05, France. Tel.: +33 310 206 2285.
E-mail address: ghil@lmd.ens.fr (M. Ghil).

0167-2789/$ - see front matter © 2008 Elsevier B.V. All rights reserved.
doi:10.1016/j.physd.2008.03.036

unlikely to ever be in equilibrium. The three successive IPCC reports (1991 [2], 1996, and 2001 [3]) concentrated therefore, in addition to estimates of equilibrium sensitivity, on estimates of climate change over the 21st century, based on several scenarios of CO_2 increase over this time interval, and using up to 18 general circulation models (GCMs) in the fourth IPCC Assessment Report (AR4) [4].

The GCM results of temperature increase over the coming 100 years have stubbornly resisted any narrowing of the range of estimates, with results for T_s in 2100 as low as 1.4 K or as high as 5.8 K, according to the Third Assessment Report. The hope in the research leading up to the AR4 was that a set of suitably defined "better GCMs" would exhibit a narrower range of year-2100 estimates, but this does not seem to have been the case.

The difficulty in narrowing the range of estimates for either equilibrium sensitivity of climate or for end-of-the-century temperatures is clearly connected to the complexity of the climate system, the multiplicity and nonlinearity of the processes and feedbacks it contains, and the obstacles to a faithful representation of these processes and feedbacks in GCMs. The practice of the science and engineering of GCMs over several decades has amply demonstrated that any addition or change in the model's "parametrizations" – *i.e.*, of the representation of subgrid-scale processes in terms of the model's explicit, large-scale variables – may result in noticeable changes in the model solutions' behavior.

As an illustration, Fig. 1 shows the sensitivity of an atmospheric GCM, which does not include a dynamical ocean, to changes in its model parameters. Several thousand simulations were performed as part of the "climate*prediction*.net" experiment [6], using perturbations in several parameters of the Hadley Centre's HadAM3 model [7], coupled to a passive, mixed-layer ocean model. The lower panel of Fig. 1 clearly illustrates a wide range of responses to CO_2 doubling, from about −1 K to about 8 K [8].

The last IPCC report [4] has investigated climate change as a result of various scenarios of CO_2 increase for a set of 18 distinct GCMs. The best estimate of the temperature increase at the end of the 21st century from AR4 is about 4.0 °C for the worst scenario of greenhouse-gas increase, namely A1F1, this scenario envisages, roughly speaking, a future world with a very rapid economic growth. The likely range of end-of-century increase in global temperatures is of 2.4–6.4 °C in this case, and comparably large ranges of uncertainties obtain for all the other scenarios as well [4]. The consequences of these scientific uncertainties for the ethical quandaries arising in the socio-economic and political decision-making process involved in adaptation to and mitigation of climate changes are discussed in [5].

An essential contributor to this range of uncertainty is natural climate variability [9] of the coupled ocean-atmosphere system. As mentioned already in [10], most GCM simulations do not exhibit the observed interdecadal variability of the oceans' buoyancy-driven, *thermohaline* circulation [11]. This circulation corresponds to a slow, pole-to-pole motion of the oceans' main water masses, also referred to as the *overturning*

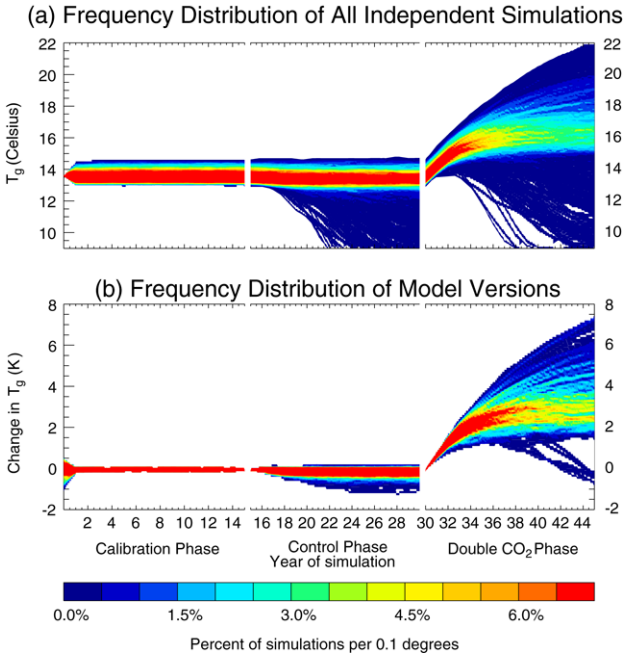

Fig. 1. Frequency distributions of global mean, annual mean, near-surface temperature (T_g) for (a) 2017 GCM simulations, and doubled CO_2; and for (b) a subset of 414 stable simulations, without substantial climate drift.

circulation. Cold and denser waters sink in the subpolar North Atlantic and lighter waters rise over much wider areas of the lower and southern latitudes.

Another striking example of low-frequency, interannual-and-interdecadal variability is provided by the near-surface, *wind-driven ocean circulation* [11,12]. Key features of this circulation are described at length in Section 2. The influence of strong thermal fronts – like the Gulf Stream in the North Atlantic or the Kuroshio in the North Pacific – on the mid-latitude atmosphere above is severely underestimated. Typical spatial resolutions in the century-scale GCM simulations of [2–4,6–8] are of the order of 100 km at best, whereas resolutions of 20 km and less would be needed to really capture the strong mid-latitude ocean-atmosphere coupling just above the oceanic fronts [13,14].

An important additional source of uncertainty comes from the difficulty to correctly parametrize global and regional effects of clouds and their highly complex small-scale physics. This difficulty is particularly critical in the tropics, where large-scale features such as the El-Niño/Southern Oscillation and the Madden–Julian oscillation are strongly coupled with convective phenomena [15–17].

The purpose of this paper is twofold. First, we describe in Section 2 the most recent theoretical results regarding the internal variability of the mid-latitude wind-driven circulation, viewed as a problem in nonlinear fluid mechanics. These results rely to a large extent on the deterministic theory of dynamical systems [18,19]. Second, we address in Section 3 the more general issue of uncertainties in climate change projections. Here we rely on concepts and methods from random dynamical systems theory [20] to help understand and possibly reduce

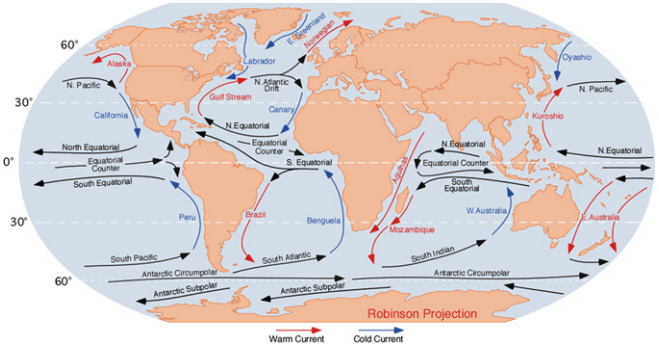

Fig. 2. A map of the main oceanic currents: warm currents in red and cold ones in blue, from http://www.physicalgeography.net..

these uncertainties. Much of the material in the latter section is new; it is supplemented by rigorous mathematical definitions and results in Appendices A and B. A summary and an outlook on future work follow in Section 4.

2. Natural variability of the wind-driven ocean circulation

2.1. Observations

To a first approximation, the main near-surface currents in the oceans are driven by the mean effect of the winds. The trade winds near the equator blow mainly from east to west and are called also the tropical easterlies. In mid-latitudes, the dominant winds are the prevailing westerlies, and towards the poles the winds are easterly again. Three of the strongest near-surface, mid-and-high-latitude currents are the Antarctic Circumpolar Current, the Gulf Stream in the North Atlantic, and the Kuroshio Extension off Japan. The Antarctic Circumpolar Current, sometimes called the Westwind Drift, circles eastward around Antarctica; see Fig. 2.

The Gulf Stream is an oceanic jet with a strong influence on the climate of eastern North America and of western Europe. Actually, the Gulf Stream is part of a larger, gyre-like current system, which includes the North Atlantic Drift, the Canary Current and the North Equatorial Current. It is also coupled with the pole-to-pole overturning circulation. From Mexico's Yucatan Peninsula, the Gulf Stream flows north through the Florida Straits and along the East Coast of the United States. Near Cape Hatteras, it detaches from the coast and begins to drift off into the North Atlantic towards the Grand Banks near Newfoundland.

The Coriolis force is responsible for the so-called Ekman transport, which deflects water masses orthogonally to the near-surface wind direction and to the right [21–23]. In the North Atlantic, this Ekman transport creates a divergence and a convergence of near-surface water masses, respectively, resulting in the formation of two oceanic gyres: a smaller, cyclonic one in subpolar latitudes, the other larger and anticyclonic in the subtropics. This type of *double-gyre* circulation characterizes all mid-latitude ocean basins, including the South Atlantic, as well as the North and South Pacific.

The double-gyre circulation is intensified as the currents approach the East Coast of North America due to the β-effect.

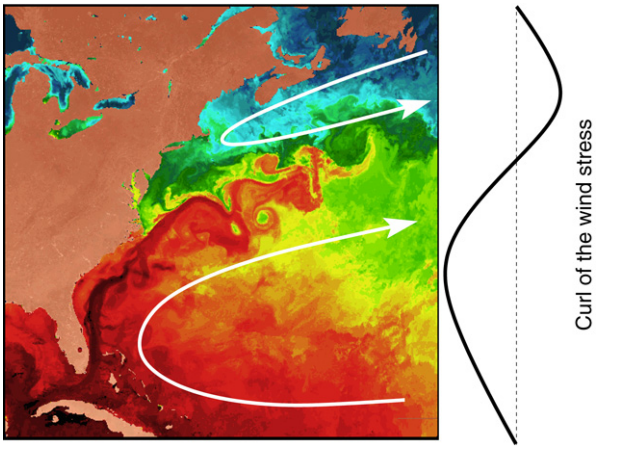

Fig. 3. A satellite image of the sea surface temperature (SST) over the northwestern North Atlantic (US National Oceanic and Atmospheric Administration), together with a sketch of the associated double-gyre circulation (white arrows). An idealized view of the amount of potential vorticity injected into the ocean circulation by the trade winds, westerlies and polar easterlies is shown to the right.

This effect arises primarily from the variation of the Coriolis force with latitude, while the oceans' bottom topography also contributes to it. The former, planetary β-effect is of crucial importance in geophysical flows and induces free Rossby waves propagating westward [21–23].

The currents along the western shores of the North Atlantic and of the other mid-latitude ocean basins exhibit boundary-layer characteristics and are commonly called western boundary currents (WBCs). The northward-flowing Gulf Stream and the southward-flowing Labrador Current extension meet near Cape Hatteras and yield a strong eastward jet. The formation of this jet and of the intense recirculation vortices near the western boundary, to either side of the jet, is mostly driven by internal, nonlinear effects.

Fig. 3 illustrates how these large-scale wind-driven oceanic flows self-organize, as well as the resulting eastward jet. Different spatial and time scales contribute to this self-organization, mesoscales eddies playing the role of the synoptic-scale systems in the atmosphere. Warm and cold rings last for several months up to a year and have a size of about 100 km; two cold rings are clearly visible in Fig. 3. Meanders involve larger spatial scales, up to 1000 km, and are associated with interannual variability. The characteristic scale of the jet and gyres is of several thousand kilometers and they exhibit their own intrinsic dynamics on time scales of several years to possibly several decades.

A striking feature of the wind-driven circulation is the existence of two well-known North-Atlantic oscillations, with a period of about 7 and 14 years, respectively. Data analysis of various climatic variables, such as sea surface temperature (SST) over the North Atlantic or sea level pressure (SLP) over western Europe [24–26] and local surface air temperatures in Central England [27], as well as of proxy records, such as tree rings in Britain, travertine concretions in southeastern France [28], and Nile floods over the last millennium or so [29], all exhibit strikingly robust oscillatory behavior with a 7-yr period

and, to a lesser extent, with a 14-yr period. Variations in the path and intensity of the Gulf Stream are most likely to exert a major influence on the climate in this part of the world [30]. This is why theoretical studies of the low-frequency variability of the double-gyre circulation are important.

Given the complexity of the processes involved, climate studies have been most successful when using not just a single model but a full hierarchy of models, from the simplest "toy" models to the most detailed GCMs [17]. In the following, we describe one of the simplest models of the hierarchy used in studying this problem.

2.2. A simple model of the double-gyre circulation

The simplest model that includes many of the mechanisms described above is governed by the barotropic *quasi-geostrophic* (QG) equations. The term geostrophic refers to the fact that large-scale rotating flows tend to run parallel to, rather than perpendicular to constant-pressure contours; in the oceans, these contours are associated with the deviation from rest of the surfaces of equal water mass, due to Ekman pumping. Geostrophic balance implies in particular that the flow is divergence-free. The term barotropic, as opposed to baroclinic, has a slightly different meaning in geophysical fluid dynamics than in engineering fluid mechanics: it means that the model describes a single fluid layer of constant density and therefore the solutions do not depend on depth [21–23].

We consider an idealized, rectangular basin geometry and simplified forcing that mimics the distribution of vorticity contribution by the winds, as sketched to the right of Fig. 3. In our idealized model, the amounts of subpolar and subtropical vorticity injected into the basin are equal and the rectangular domain $\Omega = (0, L_x) \times (0, L_y)$ is symmetric about the axis of zero wind stress curl. The barotropic two-dimensional (2-D) QG equations in this idealized setting are:

$$\begin{aligned} &q_t + J(\psi, q) - \nu\Delta^2\psi + \mu\Delta\psi = -\tau \sin\frac{2\pi y}{L_y}, \\ &q = \Delta\psi - \lambda_R^{-2}\psi + \beta y. \end{aligned} \tag{1}$$

Here q and ψ are the potential vorticity and streamfunction, respectively, and the Jacobian J corresponds to the advection of potential vorticity by the flow, $J(\psi, q) = \psi_x q_y - \psi_y q_x = \mathbf{u} \cdot \nabla q$, where $\mathbf{u} = (-\psi_y, \psi_x)$, x points east and y points north. The physical parameters are the strength of the planetary vorticity gradient β, the Rossby radius of deformation λ_R^{-2}, the eddy-viscosity coefficient ν, the bottom friction coefficient μ, and the wind-stress intensity τ. We use here free-slip boundary conditions $\psi = \Delta^2\psi = 0$; the qualitative results described below do not depend on the particular choice of homogeneous boundary conditions.

We consider (1) as an infinite-dimensional dynamical system and study its bifurcation sets as the parameters change. Two key parameters are the wind stress intensity τ and the eddy viscosity ν. An important property of (1) is its mirror symmetry in the $y = L_y/2$ axis. This symmetry can be expressed as invariance with respect to the discrete $\mathbb{Z}_2$ group $\mathcal{S}$:

$$\mathcal{S}[\psi(x, y)] = -\psi(x, L_y - y); \tag{2}$$

any solution of (1) is thus accompanied by its mirror-conjugated solution. Hence, in generic terms, the prevailing bifurcations are of either the symmetry-breaking or the saddle-node or the Hopf type.

2.3. Bifurcations in the double-gyre problem

The historical development of a comprehensive nonlinear theory of the double-gyre circulation is interesting on its own, having seen substantial progress in the last 15 years. One can distinguish four main steps.

2.3.1. Symmetry-breaking bifurcations

The first step was to realize that the first generic bifurcation of this QG model was a genuine pitchfork bifurcation that breaks the system's symmetry as the nonlinearity becomes large enough [31–33]. The situation is shown in Fig. 4. When the forcing is weak or the dissipation is large, there is only one steady solution, which is antisymmetric with respect to the mid-axis of the basin. This solution exhibits two large gyres, along with their typical, β-induced WBCs. Away from the western boundary, such a near-linear solution (not shown) is dominated by *Sverdrup* balance between wind stress curl and the meridional mass transport [21,34].

As the wind stress increases, the near-linear Sverdrup solution develops an eastward jet along the mid-axis, which penetrates farther into the domain. This more intense, and hence more nonlinear solution is still antisymmetric about the mid-axis, but loses its stability for some critical value of the wind-stress intensity (indicated by "Pitchfork" in Fig. 4).

A pair of mirror-symmetric solutions emerges and is characterized by a rather different vorticity distribution; the streamfunction fields associated with the two stable steady-state branches are plotted to the upper-left and right of Fig. 4. In particular, the jet in such a solution exhibits a large meander, reminiscent of the one seen in Fig. 3 just downstream of Cape Hatteras; note that the colors in Fig. 4 have been chosen to facilitate the comparison with Fig. 3. These asymmetric flows are characterized by one gyre being stronger in intensity than the other and therefore the jet is deflected either to the southeast or to the northeast.

2.3.2. Gyre modes

The next step was taken in part concurrently with [31,32] and in part shortly after [35–37] the first one. It involved the study of time-periodic instabilities through Hopf bifurcation from either an antisymmetric or an asymmetric steady flow. Some of these studies concentrated on the wind-driven circulation formulated for the stand-alone, single gyre [37,38]. The idea was to develop a full generic picture of the time-dependent behavior of the solutions in more turbulent regimes, by classifying the various instabilities in a comprehensive way. However, it quickly appeared that one kind of asymmetric instabilities, called *gyre modes* [32,35], was prevalent across the full hierarchy of models of the double-gyre circulation; furthermore, these instabilities trigger the lowest nonzero frequency present in these models.

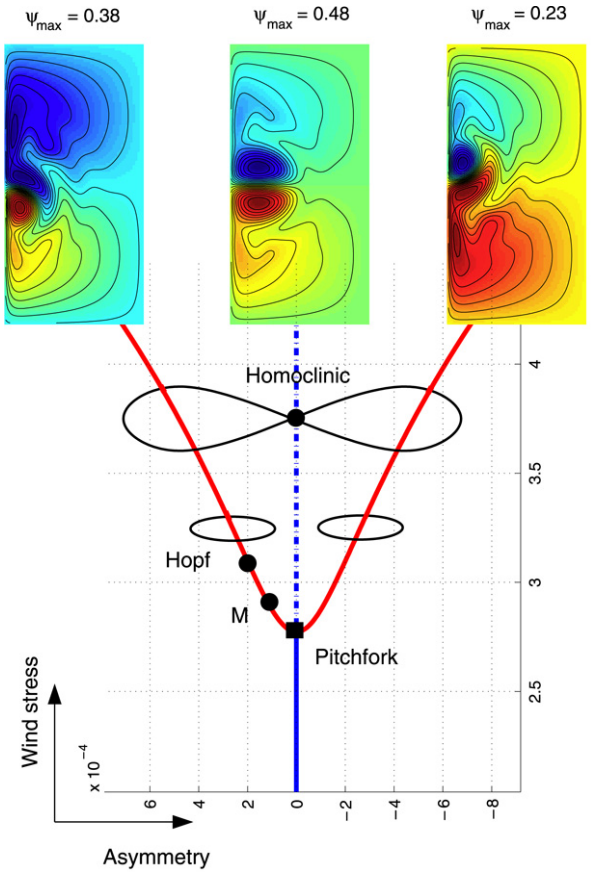

Fig. 4. Generic bifurcation diagram for the barotropic QG model of the double-gyre problem: the asymmetry of the solution is plotted versus the intensity of the wind stress τ. The streamfunction field is plotted for a steady-state solution associated with each of the three branches; positive values in red and negative ones in blue (after [46]).

These modes always appear *after* the first pitchfork bifurcation, and it took several years to really understand their genesis: gyre modes arise as two eigenvalues merge — one is associated with a symmetric eigenfunction and responsible for the pitchfork bifurcation, the other is associated with an antisymmetric eigenfunction [39]; this merging is marked by *M* in Fig. 4.

Such a phenomenon is not a bifurcation *stricto sensu*: one has topological C^0 equivalence before and after the eigenvalue merging, but not from the C^1 point of view. We recall here that functions are C^k if they and their inverses are k times continuously differentiable. Still, this phenomenon is quite common in small-dimensional dynamical systems with symmetry, as exemplified by the unfolding of codimension-2 bifurcations of Bogdanov-Takens type [19]. In particular, the fact that gyre modes trigger the lowest-frequency of the model is due to the frequency of these modes growing quadratically from zero until nonlinear saturation. Of course, these modes, in turn, become unstable shortly after the merging, through a Hopf bifurcation, indicated by "Hopf" in Fig. 4.

2.3.3. Global bifurcations

The importance of these gyre modes was further confirmed recently through an even more puzzling discovery. Several authors realized, independently of each other, that the low-frequency dynamics of their respective double-gyre models was driven by intense relaxation oscillations of the jet [40–46]. These relaxation oscillations, already described in [32,35], were now attributed to *homoclinic* bifurcations, with a global character in phase space [19,22]. In effect, the QG model reviewed here undergoes a genuine homoclinic bifurcation (see Fig. 4), which is generic across the full hierarchy of double-gyre models. Moreover, this global bifurcation is associated with chaotic behavior of the flow due to the Shilnikov phenomenon [43,46], which induces horseshoes in phase space.

The connection between such homoclinic bifurcations and gyre modes was not immediately obvious, but Simonnet et al. [46] emphasized that the two were part of a single, global dynamical phenomenon. The homoclinic bifurcation indeed results from the unfolding of the gyre modes' limit cycles. This familiar dynamical scenario is again well illustrated by the unfolding of a codimension-2 Bogdanov-Takens bifurcation, where the homoclinic orbits emerge naturally. We deal, once more, with the lowest-frequency modes, since homoclinic orbits have an infinite period. Due to the genericity of this phenomenon, it was natural to hypothesize that the gyre-mode mechanism, in this broader, global-bifurcation context, gave rise to the observed 7-yr and 14-yr North-Atlantic oscillations. Although this hypothesis may appear a little farfetched, in view of the simplicity of the double-gyre models analyzed in detail so far, it poses an interesting question.

2.3.4. Quantization and open questions

The chaotic dynamics observed in the QG models after the homoclinic bifurcation is eventually destroyed as the nonlinearity and the resolution both increase. As one expects the real oceans to be in a far more turbulent regime than those studied so far, some authors proposed different mechanisms for low-frequency variability in fully turbulent flow regimes [47,48]. It turns out, though, that – just as gyre modes could be reconciled with homoclinic-driven dynamics, – the latter can also be reconciled with eddy-driven dynamics, via the so-called *quantization* of the low-frequency dynamics [49].

Primeau [50] showed that, in large basins comparable in size with the North Atlantic, there is not only one but a set of successive pitchfork bifurcations. One supercritical pitchfork bifurcation, associated with the destabilization of antisymmetric flows, is followed generically by a subcritical one, associated this time with a stabilization of antisymmetric flows (modulo high-frequency instabilities) [49]. As a matter of fact, this phenomenon appears to be a consequence of the spectral behavior of the 2-D Euler equations [51], and hence of the closely related barotropic QG model in bounded domains.

Remarkably, this scenario repeats itself as the nonlinearity increases, but now higher wavenumbers are involved in physical space. Simonnet [49] showed that this was also the case for gyre modes and the corresponding dynamics induced by global bifurcations: the low-frequency dynamics is quantized as the jet stream extends further eastward into the basin, due to the increased forcing and nonlinearity. Fig. 5 illustrates this situation: two families of regimes can

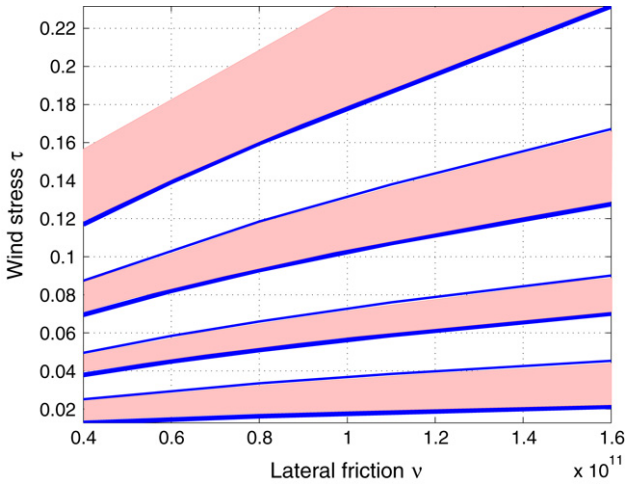

Fig. 5. Two-parameter plane, with the wind-stress intensity τ *vs.* the eddy-viscosity coefficient ν: the curves indicate the locations of supercritical and subcritical pitchfork bifurcations. Each band is associated with a different wavenumber and timescale (from [49]).

be identified, the colored bands correspond to (supercritical) regimes driven by the gyre modes, the others to (subcritical) regimes driven by the eddies. Note that this scenario is also robust to perturbing the problem's symmetry.

The successive-bifurcation theory appears therewith to be fairly complete for barotropic, single-layer models of the double-gyre circulation. This theory also provides a self-consistent, plausible explanation for the climatically important 7-year and 14-year oscillations of the oceanic circulation and the related atmospheric phenomena in and around the North-Atlantic basin [11,12,24–29,45,46]. The dominant 7- and 14-year modes of this theory also survive perturbation by seasonal-cycle changes in the intensity and meridional position of the westerly winds [52].

In baroclinic models, with two or more active layers of different density, baroclinic instabilities [11,14,21–23,30,38, 45,47,48] surely play a fundamental role, as they do in the observed dynamics of the oceans. However, it is not known to what extent baroclinic instabilities can destroy gyre-mode dynamics. The difficulty lies in a deeper understanding of the so-called *rectification* process [53], which arises from the nonzero mean effect of the baroclinic component of the flow.

Roughly speaking, rectification drives the dynamics far away from any steady states. In this situation, dynamical systems theory cannot be used as an explanation of complex, observed behavior resulting from successive bifurcations that are rooted in a simple steady state. Other tools from statistical mechanics and nonequilibrium thermodynamics should, therefore, be considered [54–57]. Combining these tools with those of the successive-bifurcation approach may eventually lead to a more general and complete physical characterization of gyre modes in realistic models.

3. Climate-change projections and random dynamical systems (RDSs)

As discussed in Section 1, the climate system's natural variability and the difficulties in parametrizing subgrid-scale processes are not the only causes for the uncertainties in projecting future climate evolution. In this section, we address more generally these uncertainties and present a novel approach for treating them. To do so, we start with some simple ideas about deterministic *vs.* stochastic modeling.

3.1. Background and motivation

Many physical phenomena can be modeled by deterministic evolution equations. Dynamical systems theory is essentially a geometric approach for studying the asymptotic, long-term properties of solutions to such equations in phase space. Pioneered by Poincaré [58], this theory took great strides over the last fifty years. To apply the theory in a reliable manner to a set of complex physical phenomena, one needs a criterion to evaluate the *robustness* of a given model within a class of dynamical systems. Such a criterion should help us deal with the inescapable uncertainties in model formulation, whether due to incomplete knowledge of the governing laws or inaccuracies in determining model parameters.

In this context, Andronov and Pontryagin [59] took a major step toward classifying dynamical systems, by introducing the concept of *structural stability*. Structural stability means that a small, continuous perturbation of a given system preserves its dynamics up to a *homeomorphism*, *i.e.*, up to a one-to-one continuous change of variables that transforms the phase portrait of our system into that of the nearby system; thus fixed points go into fixed points, limit cycles into limit cycles, etc. Closely related is the notion of *hyperbolicity* introduced by Smale [60]. A system is hyperbolic if, (very) loosely speaking, its limit set can be continuously decomposed into invariant sets that are either contracting or expanding; see [61] for more rigorous definitions.

A very simple example is the phase portrait in the neighborhood of a fixed point of saddle type. In this case, the Hartman-Grobman theorem states that the dynamics in this neighborhood is structurally stable. The converse statement, *i.e.* whether structural stability implies hyperbolicity, is still an open question; the equivalence between structural stability and hyperbolicity has only been shown in the C^1 case, under certain technical conditions [62–65]. Bifurcation theory is well grounded in the setting of hyperbolic dynamics. Problems with hyperbolicity and bifurcations arise, however, when one deals with more complicated limit sets.

Hyperbolicity was introduced initially to help pursue the "dynamicist's dream" of finding, in the abstract space of all possible dynamical systems, an open and dense set consisting of structurally stable ones. Being open and dense, roughly speaking, means that any possible dynamical system can be approximated by systems taken from this set, while systems in its complement are negligible in a suitable sense.

Smale conjectured that hyperbolic systems form an open and dense set in the space of all C^1 dynamical systems. If this conjecture were true then hyperbolicity would be typical of all dynamics. Unfortunately, though, this conjecture is only true for one-dimensional dynamics and flows on disks and surfaces [66]. Smale [67] himself found several counterexamples to

his conjecture. Newhouse [68] was able to generate open sets of nonhyperbolic diffeomorphisms using homoclinic tangencies. For the physicist, it is even more striking that the famous Lorenz attractor [69] is structurally unstable. Families of Lorenz attractors, classified by topological type, are not even countable [70,71]. In each of these examples, we observe chaotic behavior in a nonhyperbolic situation, *i.e. nonhyperbolic chaos.*

Nonhyperbolic chaos appears, therefore, to be a severe obstacle to any "easy" classification of dynamic behavior. As mentioned by Palis [65], Kolmogorov already suggested at the end of the sixties that "the global study of dynamical systems could not go very far without the use of new additional mathematical tools, like probabilistic ones". Once more, Kolmogorov showed prophetic insight, and nowadays the concept of *stochastic stability* is an important tool in the study of genericity and robustness for dynamical systems. To replace the failed program of classifying dynamical systems based on structural stability and hyperbolicity, Palis [65] formulated the following *global conjecture*: systems having only finitely many attractors (*i.e.* periodic or chaotic sinks) – such that (i) the union of their basins has full Lebesgue measure; and (ii) each is stochastically stable in their basins of attraction – are dense in the C^r, $r \geq 1$ topology. A system is stochastically stable if its Sinai–Ruelle–Bowen (SRB) measure [72] is stable with respect to stochastic perturbations, and the SRB measure is given by $\lim_{n\to\infty} \frac{1}{n} \sum_i \delta_{z_i}$, with z_i being the successive iterates of the dynamics. This measure is obtained intuitively by allowing the entire phase space to flow onto the attractor [73].

Stochastic stability is fundamentally based on ergodic theory. We would like to consider a more geometric approach, which can provide a coarser, more robust classification of GCMs and their climate-change projections. In this section, we propose such an approach, based on concepts from the rapidly growing field of random dynamical systems (RDSs), as developed by Arnold [20] and his "Bremen group", among others. RDS theory describes the behavior of dynamical systems subject to external stochastic forcing; its tools have been developed to help study the geometric properties of stochastic differential equations (SDEs). In some sense, RDS theory is the stochastic counterpart of the geometric theory of ordinary differential equations (ODEs). This approach provides a rigorous mathematical framework for a stochastic form of robustness, while the more traditional, topological concepts do not seem to be appropriate.

3.2. RDSs, random attractors, and robust classification

Stochastic parametrizations for GCMs aim at compensating for our lack of detailed knowledge on small spatial scales in the best way possible [74–79]. The underlying assumption is that the associated time scales are also much shorter than the scales of interest and, therefore, the lag correlation of the phenomena being parametrized is negligibly small. Stochastic parametrizations thus essentially transform a deterministic autonomous system into a nonautonomous one, subject to random forcing.

Explicit time dependence in a dynamical system immediately raises a technical difficulty. Indeed, the classical notion of attractor is not always relevant, since any object in phase space is "moving" with time and the natural concept of forward asymptotics is meaningless. One needs therefore another notion of attractor. In the deterministic nonautonomous framework, the appropriate notion is that of a *pullback attractor* [80], which we present below. The closely related notion of *random attractor* in the stochastic framework is also explained briefly below, with further details given in Appendix A.

3.2.1. Framework and objectives

Before defining the notion of pullback attractor, let us recall some basic facts about nonautonomous dynamical systems. Consider the ODE

$$\dot{x} = f(t, x) \tag{3}$$

on a vector space X; this space could even be infinite-dimensional, if we were dealing with partial or functional differential equations, as is often the case in fluid-flow and climate problems. Rigorously speaking, we cannot associate a dynamical system acting on X with a nonautonomous ODE; nevertheless, in the case of unique solvability of the initial-value problem, we can introduce a two-parameter family of operators $\{S(t, s)\}_{t\geq s}$ acting on X, with s and t real, such that $S(t, s)x(s) = x(t)$ for $t \geq s$, where $x(t)$ is the solution of the Cauchy problem with initial data $x(s)$. This family of operators satisfies $S(s, s) = \mathrm{Id}_X$ and $S(t, \tau) \circ S(\tau, s) = S(t, s)$ for all $t \geq \tau \geq s$, and all real s. This family of operators is called a "process" by Sell [81]. It extends the classical notion of the resolvent of a nonautonomous linear ODE to the nonlinear setting.

We can now define the pullback attractor as simply the family of invariant sets $\{\mathcal{A}(t)\}$ that satisfy for every real t and all x_0 in X:

$$\lim_{s\to-\infty} \mathrm{dist}\,(S(t, s)x_0, \mathcal{A}(t)) = 0. \tag{4}$$

"Pullback" attraction does not involve running time backwards; it corresponds instead to the idea of measurements being performed at present time t in an experiment that was started at some time $s < t$ in the past: the experiment has been running for long enough, and we are thus looking now at an "attracting state". Note that there exists several ways of defining a pullback attractor — the one retained here is a local one (*cf.* [80] and references therein); see [82] for further information on nonautonomous dynamical systems in general.

In the stochastic context, noise forcing is modeled by a stationary stochastic process. If the deterministic dynamical system of interest is coupled to this stochastic process in a reasonable way – to be expressed below by the "cocycle property" – then random pullback attractors may appear. These pullback attractors will exist for almost each sample path of the driving stochastic process, so that the same probability distribution governs both sample paths and their corresponding pullback attractors. A more detailed explanation is given in Appendix A.

Roughly speaking, this concept of *random attractor* provides a geometric framework for the description of asymptotic regimes in the context of stochastic dynamics. To compare different stochastic systems in terms of their random attractors that evolve in time, it would be nice to be able to identify the common underlying geometric structures via a random change of variables. This identification is achieved through the concept of *stochastic equivalence* that is developed in Appendix A, and it is central in obtaining a coarser and more robust classification than in the purely deterministic context.

Returning now to our main objective, suppose for instance that one is presented with results from two distinct GCMs, say two probability distributions functions (PDFs) of the temperature or precipitation in a given area. These two PDFs are generated, typically, by an ensemble of each GCM's simulations, as described in the introduction, and they are likely to differ in their spatial pattern. To ascertain the physical significance of this discrepancy, one needs to know how each GCM result varies as either a parametrization or a parameter value are changed.

In order to consider the difficult question of why GCM responses to CO_2 doubling might differ, one idea is to investigate the structure of the space of all GCMs. We mean therewith the space of all deterministic GCMs, when their stochastic parametrizations are switched off. We know, by now, from experience with GCM results over several decades – including the four IPCC assessment reports [2–4] and the climate*prediction*.net exercise [6–8] – that there is enormous scatter in this space; see also [84,85]. Our question, therefore, is: can we achieve a more robust classification of GCMs when stochastic parametrizations are used and for a given level of the noise?

As mentioned in Section 3.1, such a classification is not feasible by restricting ourself to deterministic systems and topological concepts. As one switches on stochastic parametrizations [74–79], the situation might change, and hopefully improve, dramatically: as the noise level becomes large enough, the models' deterministic behavior may be completely destroyed, and all the results could cluster into one huge, diffuse clump. We would like, therefore, to investigate how a classification based on stochastic equivalence evolves as the level of the noise or the stochastic parametrizations change. As the noise tends to zero, do we recover the "granularity" of the set of all deterministic dynamical systems? This idea is schematically represented in Fig. 6: for a given level of the noise, we expect the space of all GCMs to be decomposed into a possibly finite number of classes. Within one of these classes, all the GCMs are topologically equivalent in the stochastic sense defined above; see Eq. (A.2).

Serious difficulties might arise in this program, due to the presence of nonhyperbolic chaos in climate models. Several studies have pointed out that the characteristics of nonhyperbolic chaos in the presence of noise may depend on its intensity and statistics [86–89].

Such issues, however, go well beyond the setting of this paper and are left for further investigation. Much more modestly, we will study here whether, in certain very simple

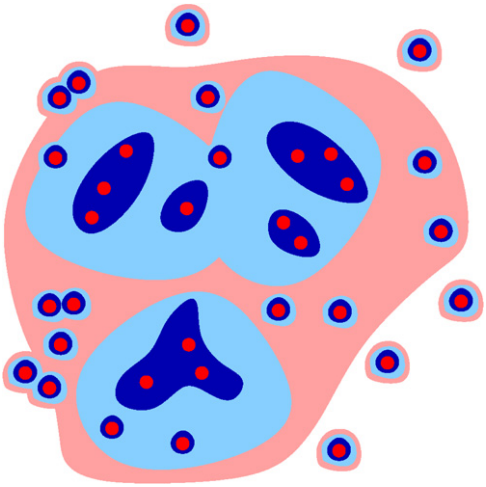

Fig. 6. A conjectural view of stochastic classification for GCMs, using the concept of random attractors. Each point in red represents a GCM in which stochastic parametrizations are switched off, while each gray area represents a cluster of stochastically equivalent GCMs for a given level of the noise.

cases, the conjectural view of Fig. 6 might be relevant for some dynamical systems that are "metaphors" of climate dynamics. The following subsection is dedicated to the study of such a metaphorical object, namely the Arnol'd circle map.

3.2.2. *The stochastically perturbed circle map*

To go beyond our pictorial view of stochastic classification for GCMs in Fig. 6, we study now the effect of noise on a family of diffeomorphisms of the circle. This toy model exhibits two features of interest for our purpose. The first one is that the two-parameter family $\{F_{\tau,\epsilon}\}$ defined by Eq. (5) below exhibits an infinite number of topological classes [18]. The second feature of interest is the frequency-locking behavior observed in many field of physics in general [90–92] and in some El-Niño/Southern-Oscillation (ENSO) models in particular [93–99]. Studying noise effects on these two features has, therefore, physical and mathematical, as well as climatological relevance.

Many physical and biological systems exhibit interference effects due to competing periodicities. One such effect is mode locking, which is due to nonlinear interaction between an "internal" frequency ω_i of the system and an "external" frequency ω_e. In the ENSO case, the external periodicity is the seasonal cycle. A simple model for systems with two competing periodicities is the well-known Arnol'd family of circle maps

$$x_{n+1} = F_{\tau,\epsilon}(x_n) := x_n + \tau - \epsilon \sin(2\pi x_n) \bmod 1, \tag{5}$$

where basically $\tau := \omega_i/\omega_e$ and ϵ parameterizes the magnitude of nonlinear effects; the map (5) is often called the *standard circle map* [18].

These maps also represent frequency locking near a bifurcation of Neimark-Sacker type (*e.g.* [100], p. 434); here the parameter τ is typically interpreted as the novel (internal) frequency involved in the bifurcation and ϵ corresponds to the nonlinearity near the bifurcation.

Such nonlinear coupling between two oscillators gives rise to a characteristic pattern, in the plane of ϵ *vs.* τ, called Arnol'd tongues. We computed this pattern numerically for the family

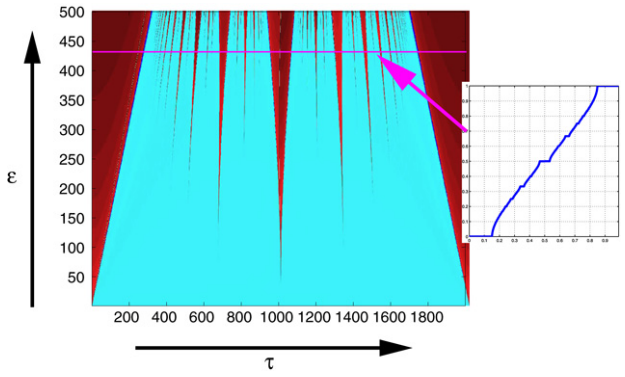

Fig. 7. Arnol'd tongues for the family of diffeomorphisms of the circle; units for τ and ϵ are 5×10^{-4} and 10^{-4} respectively. Devil's staircase in the cross-section to the right.

of Eq. (5), together with a cross-section at a fixed value of ϵ; see Fig. 7. This cross-section exhibits the so-called Devil's staircase, with "steps" on which the *rotation number* [58] is constant within each Arnol'd tongue; the rotation number measures the average rotation per iterate of (5).

For $\epsilon = 0$, two types of phenomena occur: either τ is rational and in this case the dynamics is periodic with period q, where $\tau = p/q$, or τ is irrational and the iterates $\{x_n\}$ fill the whole circle densely. As ϵ increases, an Arnol'd tongue of increasing width grows out of each $\tau = p/q$ on the abscissa $\epsilon = 0$. It follows that, in this very simple case, such an Arnol'd tongue corresponds to hyperbolic dynamics that is robust to perturbations, as verified by linearizing the map at the periodic point; the rotation number is then rational and equal to p/q.

The set of all these tongues is dense within the whole circle map family, while the Lebesgue measure of this set, at given ϵ, tends to zero as ϵ goes to zero. On the contrary, if a point in the (τ, ϵ)-plane does not belong to an Arnol'd tongue, the rotation number for those parameter values is irrational and the dynamics is nonhyperbolic; the latter fact follows, for instance, from a theorem of Denjoy [101] showing that such dynamics is smoothly equivalent to an irrational rotation. The probability to observe nonhyperbolic dynamics tends therewith to unity as ϵ goes to zero. One has, therefore, a countably infinite number of distinct topological classes, namely the Arnol'd tongues p/q, and an uncoutably infinite number of maps with irrational rotation numbers.

What happens when noise is added in Eq. (5)? We consider here the case of additive forcing by a noise process obtained via sampling at each iterate n a random variable with uniform density and intensity σ. Experiments with colored, rather than white noise and multiplicative, rather than additive noise led to the same qualitative results. The results for additive white noise are shown in Fig. 8 for three different levels of noise intensity σ.

As expected, only the largest tongues survive the presence of the noise; in particular, there is only a finite number of surviving tongues, shown in red in Fig. 8. Within such a surviving tongue, the random attractor $\mathcal{A}(\omega)$ is a random periodic cycle of period q (not shown). In the blue region outside the Arnol'd tongues, the random attractor is a fixed but random point $\mathcal{A}(\omega) = \{a(\omega)\}$: if one starts a numerical simulation for a fixed realization of the noise ω, all initial data x converge to the same fixed point a, say.

We illustrate this remarkable property in Fig. 9 in the case of a random fixed point, for given ϵ and τ. The Lyapunov exponent for the three distinct trajectories shown in the figure is strictly negative and the trajectories are exponentially attracted to the single random fixed point $a(\omega)$, the realization of the driving system $\theta(\omega)$ being the same for all the trajectories; see Appendices A and B. Kaijser [102] provided rigorous results on this type of synchronization phenomenon, but in a totally different conceptual setting. Interestingly, as the noise intensity increases, the Lyapunov exponent becomes more negative, so that the synchronization occurs even more rapidly, given a fixed realization ω.

This clustering behavior of trajectories with different initial data is in fact well known for flows on the circle [103]. In our example, this phenomenon in phase space is related to a smoothing of the Devil's staircase in parameter space, the latter cannot be solely explained by the former. Indeed, we show in Appendix B that for different irrational numbers and a sufficiently high noise level, the corresponding stochastic dynamics are stochastically equivalent, an equivalence that results in the smoothing of certain steps of the Devil's staircase.

As shown in the lower panel of Fig. 8, there is also a direct relationship between the random dynamics and the support of the PDF on the circle. For a given noise level, this support can either be the union of a finite number of disjoint intervals (red and blue curves) or it can fill the whole circle (black curve). The random attractor is, accordingly, either a random periodic orbit, with the disjoint intervals being visited in succession, or a random fixed point; this PDF behavior characterizes the level of the noise needed to destroy a given tongue.

An exact definition of random fixed point and random periodic orbit is given in Appendix B, where we provide a rigorous justification of the numerical results in Figs. 7–9. This theoretical analysis helps clarify the interaction between noise and nonlinear dynamics in the context of the GCM classification problem we are interested in.

4. Concluding remarks

We recall that Section 2 dealt with the natural, interannual and interdecadal variability of the ocean's wind-driven circulation. The oceans' internal variability is an important source of uncertainty in past-climate reconstructions and future-climate projections [9–12]. In Section 3 and Appendices A and B, we dealt more generally with the problem of structural instability as a possible cause for the stubborn tendency of the range of uncertainties in climate change projections to increase, rather than diminish over the last three decades [1–4]; see again Fig. 1. We summarize here the main results of the two sections in succession, and outline several open problems.

The wind-driven double-gyre circulation dominates the near-surface flow in the oceans' mid-latitude basins. Particular attention was paid to the North Atlantic and North Pacific, traversed by the best-known oceanic jets, namely the Gulf

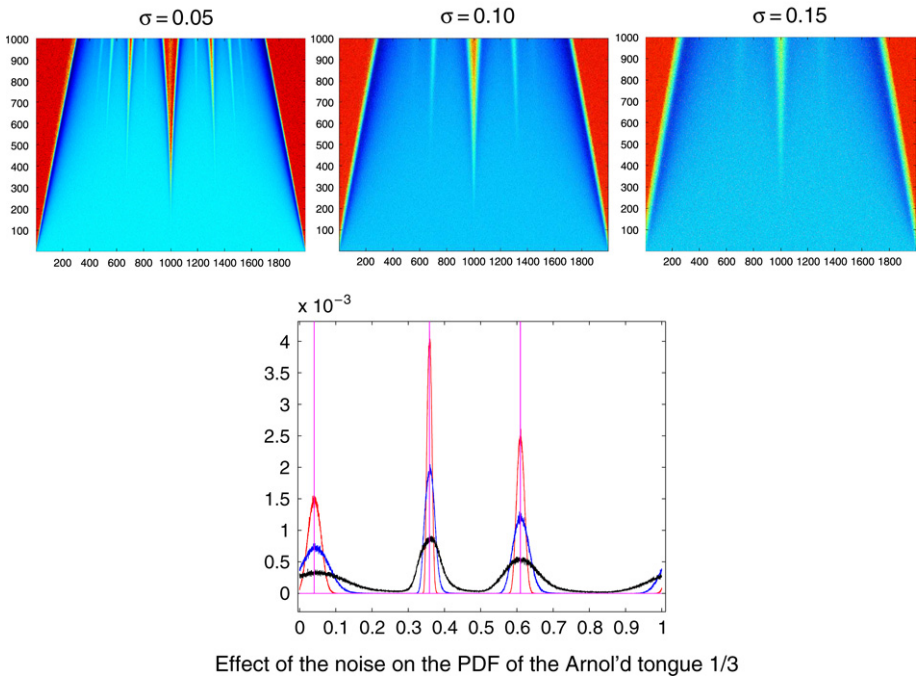

Fig. 8. Arnol'd tongues in the presence of additive noise with different noise amplitudes σ. Upper panels: Arnol'd tongues for $\sigma = 0.05, 0.10$ and 0.15; lower panel: PDF for $\epsilon = 0.9$ and the three σ-values in the upper panels: $\sigma = 0.05$ (red curve), $\sigma = 0.10$ (blue curve), and $\sigma = 0.15$ (black curve).

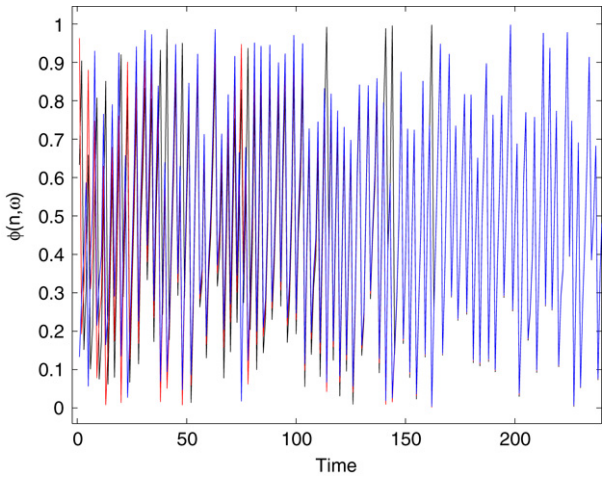

Fig. 9. Synchronization by additive noise: three distinct trajectories (in blue, red and black) of $x_{n+1} = F_{\tau,\epsilon;\omega}(x_n)$, with $F_{\tau,\epsilon;\omega}$ given by (B.1); the three trajectories start from three initial points on the circle, but are driven by the same realization ω of the noise, and thus converge to the same random fixed point $a(\omega)$, which is moving with time. The parameters are $\epsilon = 0.5$, $\tau = 0.283$ and $\sigma = 0.3$, and the corresponding Lyapunov exponent is $\lambda \simeq -0.0104$.

Stream and the Kuroshio Extension (see Fig. 2). The wind-driven circulation exhibits very rich internal dynamics and multiscale behavior associated with turbulent mesoscales (see Fig. 3). Aside from the intrinsic interest of this problem in physical oceanography, these major oceanic currents help regulate the climate of the adjacent continents, while their low-frequency variability affects past, present and future global climate.

Thanks in part to the systematic use of dynamical systems theory, a comprehensive understanding of simple, barotropic, quasi-geostrophic (QG) models of the double-gyre circulation has been achieved over the last two decades, and was reviewed in Section 2 here. In particular, the importance of symmetry-breaking and homoclinic bifurcations (see Fig. 4) in explaining the observed low-frequency variability has been validated across a wide hierarchy of models, including models with much more comprehensive physical formulation, more realistic geometry, and greater resolution in the horizontal and vertical [11,12]. This successive-bifurcation theory also provides a self-consistent explanation for the climatically important 7-year and 14-year oscillations of the oceanic circulation and the related atmospheric phenomena in and around the North-Atlantic basin [11,12,24–29,45,46].

The next challenge in physical oceanography is to reconcile the points of view of dynamical systems theory and statistical mechanics in describing the interaction between the largest scales of motion and geostrophic mesoscale turbulence, which is fully captured in baroclinic QG models. We emphasize that the complexity of these models of the double-gyre circulation is intermediate between high-end GCMs and simple "toy" models; these models offer, therefore, an ideal laboratory to test our ideas. In particular, stochastic parametrizations of the rectification process, absent in barotropic QG models, could be studied using some of the concepts and tools from RDS theory presented here. Note that the RDS approach has already been used in the context of stochastic partial differential equations, in particular for showing the existence of random attractors, as well as stable, unstable and inertial manifolds. Thus RDS concepts and tools are not restricted to finite-dimensional systems [104–106].

In Section 3, we have addressed the range-of-uncertainty problem for IPCC-class GCM simulations (see Fig. 1) by considering them as stochastically perturbed dynamical

systems. This approach is consonant with recent interest for stochastic parametrizations in the high-end modeling-and-simulation community [74–79]. Rigorous mathematical results from the dynamical systems literature suggest that – in the absence of stochastic ingredients – GCMs as well as simpler models, found on the lower rungs of the modeling hierarchy [17], are bound to differ from each other in their results.

This sensitivity follows from the fact that, among deterministic dynamical systems, those that are hyperbolic are essentially the only ones that are also structurally stable, at least in the C^1 case [62–65]. Thus, because hyperbolic systems are not dense in the set of smooth deterministic ones [67], we are led to conclude that the topological, structural-stability approach does not guarantee deterministic-model robustness, in spite of its many valuable contributions so far. Related issues for GCM modeling were emphasized recently by Mitchell [83], Held [84] and McWilliams [85].

We have gone one step further and considered model robustness in the presence of stochastic terms; such terms could represent either parametrizations of unresolved processes in GCMs or stochastic components of natural or anthropogenic forcing, such as volcanic eruptions or fluctuations in greenhouse gas or aerosol emissions. Despite the obvious gap between idealized models and high-end simulations, we have brought to bear random dynamical systems (RDS) theory [20] on the former.

In this framework, we have considered a robustness criterion that could replace structural stability, through the concept of stochastic conjugacy (see Figs. A.1 and A.2). We have shown, for a stochastically perturbed Arnol'd family of circle maps, that noise can enhance model robustness. More precisely, this circle map family exhibits structurally stable, as well as structurally unstable behavior. When noise is added, the entire family exhibits *stochastic* structural stability, based on the stochastic-conjugacy concept, even in those regions of parameter space where deterministic structural instability occurs for vanishing noise (see Figs. 7 and 8).

Clearly the hope that noise can smooth the very highly structured pattern of distinct behavior types for climate models, across the full hierarchy, has to be tempered by a number of caveats. First, serious questions remain at the fundamental, mathematical level about the behavior of nonhyperbolic chaotic attractors in the presence of noise [86–88]. Likewise, the case of driving by nonergodic noise is being actively studied [107–109].

Second, the presence of certain manifestations of a Devil's staircase has been documented across the full hierarchy of ENSO models [17,93–99], as well as in certain observations [17,99]. Interestingly, both GCMs and observations only exhibit a few, broad steps of the staircase, such as $4:1=4$ yr, $4:2=2$ yr, and $4:3\cong 16$ months. Does this result actually support the idea that nature and its detailed models always provide sufficient noise to achieve considerable smoothing of the much finer structure apparent in simpler models? Be that as it may, we need a much better understanding of how different types of noise – additive and multiplicative, white and colored – act across even a partial hierarchy of models, say from the simplest ones, like those studied in Section 3, to the intermediate ones considered in Section 2.

Third, one needs to connect more closely the nature of a stochastic parametrization and its effects on the model's behavior in phase-parameter space. As shown in Appendix B, not all types of noise are equal with respect to these effects. We are thus left with a rich, and hopefully fruitful, set of questions, which we expect to pursue in future work.

Acknowledgements

It is a pleasure to thank the organizers and participants of the Conference on the "*Euler Equations: 250 Years On*" and, more than all, Uriel Frisch, for a stimulating and altogether pleasant experience. We are grateful to I.M. Held, J.C. McWilliams, J.D. Neelin and I. Zaliapin for many useful discussions and their continuing interest in the questions studied here. A. Sobolevskiĭ, E. Tziperman and an anonymous reviewer have provided constructive criticism and stimulating remarks that helped improve the presentation. This study was supported by the US Department of Energy grant DE-FG02-07ER64439 from its Climate Change Prediction Program, and by the European Commission's No. 12975 (NEST) project "Extreme Events: Causes and Consequences (E2-C2)".

Appendix A. RDSs and random attractors

We present here briefly the mathematical concepts and tools of random dynamical systems, random attractors and stochastic equivalence. We shall use the concept of pullback attractor introduced in Section 3.2.1 to define the closely related notion of a random attractor, but need first to define an RDS. We denote by $\mathbb{T}$ the set $\mathbb{Z}$, for maps, or $\mathbb{R}$, for flows. Let $(X, \mathcal{B})$ be a measurable phase space, and $(\Omega, \mathcal{F}, \mathbb{P}, (\theta(t))_{t\in\mathbb{T}})$ be a *metric* dynamical system *i.e.* a flow in the probability space $(\Omega, \mathcal{F}, \mathbb{P})$, such that $(t, \omega) \mapsto \theta(t)\omega$ is measurable and $\theta(t) : \Omega \to \Omega$ is measure preserving, *i.e.* $\theta(t)\mathbb{P} = \mathbb{P}$.

Let $\varphi : \mathbb{T}\times\Omega\times X \to X, (t, \omega, x) \mapsto \varphi(t, \omega)x$, be a mapping with the two following properties:

(R_1) : $\varphi(0, \omega) = \mathrm{Id}_X$, and
(R_2) (the cocycle property): For all $s, t \in \mathbb{T}$ and all $\omega \in \Omega$,

$$\varphi(t + s, \omega) = \varphi(t, \theta(s)\omega) \circ \varphi(s, \omega).$$

If φ is measurable, it is called a *measurable* RDS over θ. If, in addition, X is a topological space (respectively a Banach space), and φ satisfies $(t, \omega) \mapsto \varphi(t, \omega)x$ continuous (resp. C^k, $1 \le k \le \infty$) for all $(t, \omega) \in \mathbb{T}\times\Omega$, then φ is called a *continuous* (resp. C^k) RDS over the flow θ. If so, then

$$(\omega, x) \mapsto \Theta(t)(x, \omega) := (\theta(t)\omega, \varphi(t, \omega)x), \tag{A.1}$$

is a (measurable) flow on $\Omega \times X$, and is called the *skew-product* of θ and φ. In the sequel, we shall use the terms "RDS" or "cocycle" synonymously.

The choice of the so-called *driving system* θ is a crucial step in this set-up; it is mostly dictated by the fact that the coupling

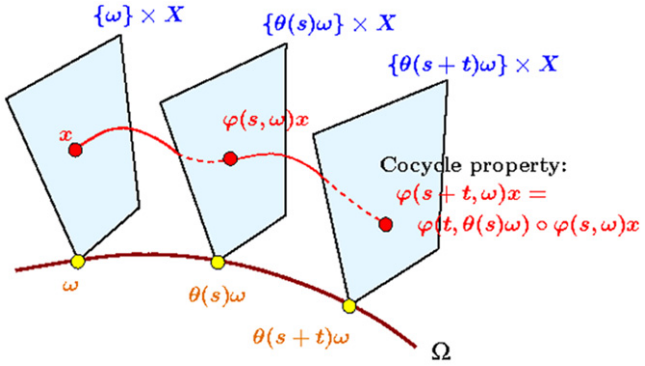

Fig. A.1. Random dynamical systems (RDS) viewed as a flow on the bundle $X \times \Omega$ = "dynamical space" × "probability space". For a given state x and realization ω, the RDS φ is such that $\Theta(t)(x, \omega) = (\theta(t)\omega, \varphi(t, \omega)x)$ is a flow on the bundle.

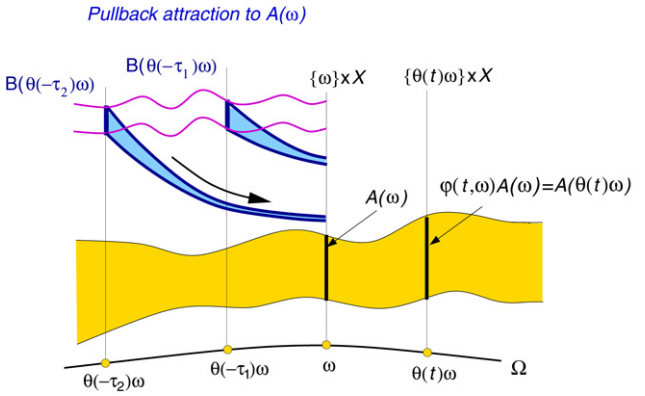

Fig. A.2. Schematic diagram of a random attractor $\mathcal{A}(\omega)$, where $\omega \in \Omega$ is a fixed realization of the noise. To be attracting, for every set B of X in a family $\mathfrak{B}$ of such sets, one must have $\lim_{t\to+\infty} \mathrm{dist}(B(\theta(-t)\omega), \mathcal{A}(\omega)) = 0$ with $B(\theta(-t)\omega) := \varphi(t, \theta(-t)\omega)B$; to be invariant, one must have $\varphi(t, \omega)\mathcal{A}(\omega) = \mathcal{A}(\theta(t)\omega)$. This definition depends strongly on $\mathfrak{B}$; see [112] for more details.

between the stationary driving and the deterministic dynamics should respect the time invariance of the former, as illustrated in Fig. A.1. The driving system θ also plays an important role in establishing *stochastic conjugacy* [110] and hence the kind of classification we aim at.

The concept of *random attractor* is a natural and straightforward extension of the definition of pullback attractor (4), in which Sell's [81] process is replaced by a cocycle, *cf.* Fig. A.1, and the attractor $\mathcal{A}$ now depends on the realization ω of the noise, so that we have a family of random attractors $\mathcal{A}(\omega)$, *cf.* Fig. A.2. Roughly speaking, for a fixed realization of the noise, one "rewinds" the noise back to $t \to -\infty$ and lets the experiment evolve (forward in time) towards a possibly attracting set $\mathcal{A}(\omega)$; the driving system θ enables one to do this rewinding without changing the statistics, cf. Figs. A.1 and A.2.

Other notions of attractor can be defined in the stochastic context, in particular based on the original SDE; see [111] or [112] for a discussion on this topic. The present definition, though, will serve us well.

Having defined RDSs and random attractors, we now introduce the notion of *stochastic equivalence* or *conjugacy*, in order to rigourously compare two RDSs; it is defined as follows: two cocycles $\varphi_1(\omega, t)$ and $\varphi_2(\omega, t)$ are conjugated if and only if there exists a random homeomorphism $h \in \mathrm{Homeo}(X)$ and an invariant set such that $h(\omega)(0) = 0$ and

$$\varphi_1(\omega, t) = h(\theta(t)\omega)^{-1} \circ \varphi_2(\omega, t) \circ h(\omega). \tag{A.2}$$

Stochastic equivalence extends classic topological conjugacy to the bundle space $X \times \Omega$, stating that there exists a one-to-one, stochastic change of variables that continuously transforms the phase portrait of one sample system in X into that of any other such system.

Appendix B. Coarse-graining of the circle map family

We provide here a rigorous justification of the numerical results obtained in Section 3.2.2 on the topological classification of the family of Arnol'd circle maps in the presence of noise. Consider the following random family of diffeomorphisms:

$$F_{\tau,\epsilon;\omega}(x) := x + \tau + \sigma\omega - \epsilon \sin(2\pi x) \mod 1, \tag{B.1}$$

for $x \in \mathbb{S}^1$, ϵ a real parameter in $(0, 1)$, and ω a random parameter distributed in the compact interval $I = [-1/2, 1/2]$ with fixed distribution ν and noise intensity σ. We denote by $F_{\tau,\epsilon}$ the corresponding deterministic family of diffeomorphisms when the noise is switched off, $\sigma = 0$.

In the RDS framework, we need to specify the metric dynamical system modeling the noise. We choose here the interval σI as the base for the probability space Ω and define the flow θ simply as mapping the point ω into its successor in a sequence of realizations of the noise. One could also use an irrational rotation on Ω for instance; in either case, ergodicity is ensured.

For the sake of simplicity, we omit for the moment the dependence on τ and ϵ. In discrete time, with $\mathbb{T} = \mathbb{Z}$, we define a map $\phi : \mathbb{T} \times \Omega \times \mathbb{S}^1 \to \mathbb{S}^1$, $(n, \omega, x) \mapsto \phi(n, \omega)x$, such that

$$\phi(n, \omega) := \begin{cases} F_{\theta^{n-1}\omega} \circ \cdots \circ F_{\omega}, & n \geq 1, \\ \mathrm{Id}_{\mathbb{S}^1}, & n = 0, \\ F^{-1}_{\theta^{n}\omega} \circ \cdots \circ F^{-1}_{\theta^{-1}\omega}, & n \leq -1. \end{cases} \tag{B.2}$$

One can prove easily that this ϕ satisfies the cocycle property and is in fact a C^∞ RDS on $\mathbb{S}^1$ over θ.

The pair of mappings $\Theta := (\theta, \phi)$ is the corresponding skew-product (A.1), and it defines a flow on $\Omega \times \mathbb{S}^1$ by the relation:

$$(\omega, x) \mapsto \Theta(n)(\omega, x) := (\theta^n\omega, \phi(n, \omega)x). \tag{B.3}$$

A stationary measure m on $\mathbb{S}^1$ under the random diffeomorphism $F_{\tau,\epsilon;\omega}$ yields a Θ-invariant measure $\mu := m \times \nu$, *i.e.* $\Theta_n\mu = \mu$; explicitly,

$$\int_{\Omega\times\mathbb{S}^1} f(\omega, x)\mu(\mathrm{d}\omega, \mathrm{d}x) = \int_{\Omega\times\mathbb{S}^1} f(\theta_n\omega, \phi(n, \omega)x)\mu(\mathrm{d}\omega, \mathrm{d}x) \tag{B.4}$$

for all $n \in \mathbb{T}$ and $f \in L^1(\Omega \times \mathbb{S}^1, \mu)$.

Let us recall the following important proposition [113] concerning the stationary measures obtained from the random family $\{F_{\tau,\epsilon;\omega}\}$.

Theorem 1. *The random circle diffeomorphism $F_{\tau,\epsilon;\omega}$ has a unique stationary measure $m_{\tau,\epsilon}$. The support of $m_{\tau,\epsilon}$ consists either of q mutually disjoint intervals or of the entire circle $\mathbb{S}^1$. The density function $\phi_{\tau,\epsilon}$ is in $C^\infty(\mathbb{S}^1)$ and depends C^∞ on τ. The invariant measure μ is ergodic. If the support of m is connected, then it is mixing and so is μ.*

Mixing for m means that, for any bounded function $f : \mathbb{S}^1 \to \mathbb{R}$, and for an arbitrary initial point $x_0 \in \mathbb{S}^1$, $\mathbb{E} f(\phi(n,\omega)x_0)$ tends to $\int_{\mathbb{S}^1} f(x)m(\mathrm{d}x)$ as $n \to +\infty$; see [114] for more on random attractors and mixing.

For deterministic diffeomorphisms of the circle, the rotation number measures the average rotation per iterate of $F_{\tau,\epsilon}$. In the presence of noise, one can still define a rotation number for $F_{\tau,\epsilon;\omega}$, namely

$$\rho_{\tau,\epsilon;\omega}(x) = \lim_{k\to\infty} \frac{\tilde{F}^k_{\tau,\epsilon;\omega}(x) - x}{k}, \tag{B.5}$$

where $\tilde{F}$ denotes the lift of a map F, acting on $\mathbb{S}^1$ modulo 1, to a map acting on $\mathbb{R}$. For fixed τ and ϵ, we can then show that $\rho_{\tau,\epsilon;\omega}$ exists for ν-almost all ω and is a constant; this constant $\rho_{\tau;\omega}$ is independent of x and ω [113]. Furthermore, $\tau \to \rho_{\tau,\epsilon}$ is C^∞ for each ϵ, which is not true in the deterministic case with $\sigma = 0$; see again [113].

Theorem 1 has a natural geometric counterpart in terms of random attractors, as confirmed through our numerical study; see again Fig. 8. More precisely, we introduce also the following definitions of *random fixed point* and *random periodic orbit*; these definitions differ somewhat from those given in [113].

Definition 1. A random fixed point is a measurable map $a : \Omega \to \mathbb{S}^1$ for which

$$\phi(1,\omega)a(\omega) = a(\theta(\omega)), \tag{B.6}$$

for ν-almost all $\omega \in \Omega$, *i.e.* such that $\Omega \times a(\Omega)$ is an invariant set for the flow given by the skew-product Θ. A random periodic orbit of period q is likewise an invariant set with cardinality q in fibers $\mathbb{S}^1 \times \{\omega\}$ for ν-almost all ω.

With these definitions, the following results of [113] still hold.

Theorem 2. *For a random diffeomorphism $F_{\tau,\epsilon;\omega}$ of the circle $\mathbb{S}^1$, with a stationary measure m supported on a union E of q disjoint intervals, the corresponding skew-product Θ restricted to E has precisely one attracting random periodic orbit and one repelling random periodic orbit.*

Attraction in the preceding theorem means that $\lim_{n\to\infty} |F^n_\omega(x) - F^n_\omega(a(\omega))| = 0$, for a set of initial data $(x,\omega) \in \mathbb{S}^1 \times \Omega$ with positive $\lambda \times \nu$-measure, in the case of a random attracting fixed point; here λ is Lebesgue measure on $\mathbb{S}^1$ and the extension to a random periodic orbit is obvious.

Using these two theorems and rigorous results on random point attractors [112], we can show that (i) if the support of the stationary measure is the whole circle (black curve in Fig. 8), then there exists one random fixed point which is pullback attracting; and (ii) if the support consists of q disjoint intervals, then the random attractor is a random periodic orbit of period q (red and blue curves).

Having explained how the connectedness of the PDF support at different noise levels is related to the nature of the random attractor, we now turn to an explanation of the "disappearance" of the smaller steps in the Devil's staircase, as the noise level increases. To do so, we consider the Lyapunov spectrum of an RDS, which still relies on the Oseledets [115] *multiplicative ergodic theorem* (MET).

To state an MET for RDS on manifolds, we differentiate $\phi(n,\omega)$ at $x \in \mathbb{S}^1$, and obtain the linear map

$$T\phi(n,\omega,x) : T_xM \to T_{\phi(n,\omega)x}M, \tag{B.7}$$

where $T\phi$ is a continuous linear cocycle on the tangent bundle TM of the manifold M over the skew-product flow Θ. If the flow ϕ possesses an ergodic invariant measure μ such that the required integrability condition for applying the MET is verified with respect to μ, then the MET holds for ϕ over M [116].

Because of Theorem 1 here, we can apply the MET to our problem and conclude that a unique Lyapunov exponent exists for the *linearization* of each diffeomorphism belonging to our family of random diffeomorphisms, and that this exponent is independent of the realization of the noise. We show next how to use the Lyapunov spectrum in studying the stochastic equivalence classes of a given RDS family, along with its driving system θ. This last aspect of the classification problem is outlined for linear hyperbolic cocycles.

Cong [117] has shown that, even in the linear context, the main difference with respect to the deterministic case is that the classification depends strongly on the properties of θ, which is directly linked to the system noise and its modeling. For instance, if θ is an irrational rotation on $\mathbb{S}^1$, one can construct infinitely many classes of hyperbolic cocycles that are not pairwise topologically equivalent, by playing essentially with the orientations of the cocyles, *i.e.* reversing between clockwise and anticlockwise rotation on $\mathbb{S}^1$. As we shall see, such difficulties can be avoided in the case of noisy Arnol'd tongues, especially for additive noise. Related issues still form an active research area in RDS theory; see [116] for a brief survey.

A key ingredient for the linear classification is the notion of *coboundary*, which we recall herewith.

Definition 2. A measurable set $K \subset \Omega$ is called a *coboundary* if there exists a set $H \in \mathcal{F}$ such that $K = H \triangle \theta H$, where $H \triangle \theta H$ denotes the symmetric difference of H and θH.

Let A and B be two linear random maps on $\mathbb{R}^d$, and denote by deg $A(\omega)$ and deg $B(\omega)$ the degrees of the maps $A(\omega)$ and $B(\omega)$ with respect to a chosen random orientation. These degrees are just the sign of the determinant of the corresponding random matrices, and equal -1 or 1; see [110,117] for details.

Consider the two linear hyperbolic cocycles Φ_A and Φ_B, associated with the maps A and B, and the following subset of Ω:

$$C_{AB} = \{\omega \in \Omega | \deg A(\omega) \cdot \deg B(\omega) = -1\}; \tag{B.8}$$

C_{AB} is just the set of all $\omega \in \Omega$ for which the degrees of the two linear maps $A(\omega)$ and $B(\omega)$ differ.

The main theorem for the classification of our diffeomorphisms of $\mathbb{S}^1$ follows [117].

Theorem 3. *Two one-dimensional linear hyperbolic cocycles Φ_A and Φ_B are conjugate if and only if the following conditions hold:*

(i) *sign λ_A = sign λ_B, and*
(ii) *the associated set C_{AB} is a coboundary.*

Here λ_A and λ_B indicate the Lyapunov exponents of Φ_A and Φ_B, respectively.

Before applying this result, let us explain heuristically how a Devil's staircase step that corresponds to a rational rotation number can be "destroyed" by a sufficiently intense noise. Consider the period-1 locked state in the deterministic setting. At the beginning of this step, a pair of fixed points is created, one stable and the other unstable. As the bifurcation parameter is increased, these two points move away from each other, until they are π radians apart. Increasing the parameter further causes the fixed points to continue moving along, until they finally meet again and are annihilated in a *saddle-node bifurcation*, thus signaling the end of the locking interval.

When noise is added, we have to distinguish between a "strongly locked" regime, where the stable and unstable fixed points are nearly π radians apart, and a "weakly locked" regime, where these two fixed points are close to each other. In both regimes, the relaxation time in the vicinity of the stable point represents an important time scale of the problem. In the strongly locked regime, this is the only time scale of interest. In the weakly locked regime, though, the process of escaping across the unstable fixed point is non-negligible and the associated escape time becomes the second time scale of interest. From these heuristic considerations it follows that the distinction between strong and weak locking depends on the strength of the external noise.

If we consider period-T locked states, with $T \geq 2$, the same kind of reasoning can be applied to the stable and unstable T-cycle. We conclude therefore, for a fixed $\epsilon > 0$, that the narrower Devil's staircase steps are the least robust, while the wider ones are the most robust.

The fact that a locked case becomes unlocked when noise is growing implies in particular that the rotation number $\rho_{\tau,\epsilon}$ becomes *irrational* for a sufficiently high noise level. According to Theorem 2.1 of [102], the Lyapunov exponent is strictly *negative* in this case almost surely. Moreover, by reinterpreting other results of Kaijser [102] in our RDS framework, we can show that the random attractor is in fact a random fixed point; this, in turn, allows us to conclude that the corresponding linearized cocycle at this random fixed point is hyperbolic. Next, by using the Hartman-Grobman theorem for RDSs [118–120], we can conjugate the nonlinear cocycle with its linearization; in fact, Theorem 3.1 of [119] says that this conjugacy is global.

Consider now two linearized cocycles Φ_A and Φ_B, at one and the same or at two distinct random fixed points of the family of random diffeomorphisms, for the same noise intensity, and denote by $A(\omega)$ and $B(\omega)$ the random linear parts of the cocycles Φ_A and Φ_B respectively; it follows from our model of noisy circle maps that C_{AB} is empty. Indeed, the noise being additive, the random orientation is preserved for different parameter values. But θ is assumed to be ergodic, and so we have that $\Omega \triangle \theta\Omega$ is empty and, therefore, C_{AB} is a coboundary. Therewith, Theorem 3 can be applied to obtain the desired result for the problem considered here: with an appropriate amount of noise, two deterministic diffeomorphisms that are not topologically equivalent can fall into the same topological stochastic class! The numerical results of Section 3.2 are entirely in agreement with this assertion.

Note that the set C_{AB} could differ from a coboundary, if the noise occurred additively in the phase of the nonlinear term, for instance. Here we see the importance of noise modeling in obtaining the conjectural view of Fig. 6 for a family of dynamical systems in general.

It follows, in particular, that the exact nature of the stochastic parametrizations in a family of GCMs does matter. It's not enough to follow the trend by devising and implementing such parametrizations: one should test that a given parametrization, once found to be suitable in other respects, does improve the proximity, in an appropriate sense, between climate simulations within the family of GCMs for which it has been been developed.

References

[1] J. Charney, et al., Carbon Dioxide and Climate: A Scientific Assessment, National Academies Press, Washington, DC, 1979.
[2] J.T. Houghton, G.J. Jenkins, J.J. Ephraums (Eds.), Climate Change, The IPCC Scientific Assessment, Cambridge Univ. Press, Cambridge, MA, 1991, p. 365.
[3] J.T. Houghton, Y. Ding, D.J. Griggs, M. Noguer, P.J. van der Linden, X. Dai, K. Maskell, C.A. Johnson (Eds.), Climate Change 2001: The Scientific Basis. Contribution of Working Group I to the Third Assessment Report of the Intergovernmental Panel on Climate Change (IPCC), Cambridge University Press, Cambridge, UK, 2001, p. 944.
[4] S. Solomon, D. Qin, M. Manning, Z. Chen, M. Marquis, K.B. Averyt, M. Tignor, H.L. Miller (Eds.), Climate Change 2007: The Physical Science Basis. Contribution of Working Group I to the Fourth Assessment Report of the IPCC, Cambridge University Press, Cambridge, UK and New York, NY, USA, 2007.
[5] R. Hillerbrand, M. Ghil, Anthropogenic climate change: Scientific uncertainties and moral dilemmas, Physica D 237 (14–17) (2008) 2132–2138.
[6] M.R. Allen, Do-it-yourself climate prediction, Nature 401 (1999) 627.
[7] V.D. Pope, M. Gallani, P.R. Rowntree, R.A. Stratton, The impact of new physical parameterisations in the Hadley Centre climate model - HadAM3, Clim. Dyn. 16 (2000) 123–146.
[8] D.A. Stainforth, et al., Uncertainty in predictions of the climate response to rising levels of greenhouse gases, Nature 433 (2005) 403–406.
[9] D.G. Martinson, K. Bryan, M. Ghil, et al. (Eds.), National Research Council, Natural Climate Variability on Decade-to-Century Time Scales, National Academies Press, Washington, DC, 1995, p. 630.
[10] M. Ghil, Hilbert problems for the geosciences in the 21st century, Nonlin. Proc. Geophys. 8 (2001) 211–222.

[11] H.A. Dijkstra, M. Ghil, Low-frequency variability of the large-scale ocean circulation: A dynamical systems approach, Rev. Geophys. 43 (2005) RG3002. doi:10.1029/2002RG000122.
[12] H.A. Dijkstra, Nonlinear Physical Oceanography: A Dynamical Systems Approach to the Large Scale Ocean Circulation and El Niño, 2nd ed., Springer, 2005, p. 532.
[13] Y. Feliks, M. Ghil, E. Simonnet, Low-frequency variability in the mid-latitude atmosphere induced by an oceanic thermal front, J. Atmos. Sci. 61 (2004) 961–981.
[14] Y. Feliks, M. Ghil, E. Simonnet, Low-frequency variability in the mid-latitude baroclinic atmosphere induced by an oceanic thermal front, J. Atmos. Sci. 64 (2007) 97–116.
[15] R.A. Madden, P.R. Julian, Observations of the 40–50-day tropical oscillations — a review, Monthly Weather Rev. 122 (5) (1994) 814–837.
[16] J.D. Neelin, D.S. Battisti, A.C. Hirst, F.-F. Jin, Y. Wakata, T. Yamagata, S. Zebiak, ENSO theory, J. Geophys. Res. 103 (C7) (1998) 14261–14290.
[17] M. Ghil, A.W. Robertson, Solving problems with GCMs: General circulation models and their role in the climate modeling hierarchy, in: D. Randall (Ed.), General Circulation Model Development: Past, Present and Future, Academic Press, San Diego, 2000, pp. 285–325.
[18] V.I. Arnol'd, Geometrical Methods in the Theory of Differential Equations, Springer, 1983, p. 334.
[19] J. Guckenheimer, P. Holmes, Nonlinear Oscillations, Dynamical Systems and Bifurcations of Vector Fields, 2nd ed., Springer-Verlag, 1991, p. 453.
[20] L. Arnold, Random Dynamical Systems, Springer-Verlag, 1998, p. 616.
[21] A.E. Gill, Atmosphere-Ocean Dynamics, Academic Press, 1982, p. 662.
[22] M. Ghil, S. Childress, Topics in Geophysical Fluid Dynamics: Atmospheric Dynamics, Dynamo Theory, and Climate Dynamics, Springer-Verlag, Berlin, Heidelberg, New York, 1987, p. 512.
[23] J. Pedlosky, Geophysical Fluid Dynamics, 2nd ed., Springer-Verlag, 1987, p. 710.
[24] V. Moron, R. Vautard, M. Ghil, Trends, interdecadal and interannual oscillations in global sea-surface temperatures, Clim. Dyn. 14 (1998) 545–569.
[25] C. Wunsch, The interpretation of short climate records, with comments on the North Atlantic and Southern Oscillations, Bull. Am. Meteorol. Soc. 80 (1999) 245–255.
[26] E.D. Da Costa, A.C. Colin de Verdière, The 7.7 year North Atlantic oscillation, Q. J. R. Meteorol. Soc. 128 (2004) 797–818.
[27] G. Plaut, M. Ghil, R. Vautard, Interannual and interdecadal variability in 335 years of Central England temperatures, Science 268 (1995) 710–713.
[28] M. Dubar, Approche climatique de la période romaine dans l'est du Var : recherche et analyse des composantes périodiques sur un concrétionnement centennal (Ier-IIe siècle apr. J.-C.) de l'aqueduc de Fréjus, Archeoscience 30 (2006) 163–171.
[29] D. Kondrashov, Y. Feliks, M. Ghil, Oscillatory modes of extended Nile River records (A.D. 622–1922), Geophys. Res. Lett. 32 (2005) L10702. doi:10.1029/2004GL022156.
[30] H. Stommel, The Gulf Stream: A Physical and Dynamical Description, 2nd ed., Cambridge Univ. Press, London, 1965, p. 248.
[31] S. Jiang, F.F. Jin, M. Ghil, The nonlinear behavior of western boundary currents in a wind-driven, double-gyre, shallow-water model, in: Ninth Conf. Atmos. & Oceanic Waves and Stability (San Antonio, TX), American Meterorological Society, Boston, Mass, 1993, pp. 64–67.
[32] S. Jiang, F.F. Jin, M. Ghil, Multiple equilibria, periodic, and aperiodic solutions in a wind-driven, double-gyre, shallow-water model, J. Phys. Oceanogr. 25 (1995) 764–786.
[33] P. Cessi, G.R. Ierley, Symmetry-breaking multiple equilibria in quasigeostrophic, wind-driven flows, J. Phys. Oceanogr. 25 (6) (1995) 1196–1205.
[34] H.U. Sverdrup, Wind-driven currents in a baroclinic ocean; with application to the equatorial currents of the eastern Pacific, Proc. Natl. Acad. Sci. USA 33 (1947) 318–326.
[35] S. Speich, H.A. Dijkstra, M. Ghil, Successive bifurcations in a shallow-water model applied to the wind-driven ocean circulation, Nonl. Proc. Geophys. 2 (1995) 241–268.
[36] H.A. Dijkstra, C.A. Katsman, Temporal variability of the wind-driven quasi-geostrophic double gyre ocean circulation: Basic bifurcation diagrams, Geophys. Astrophys. Fluid Dyn. 85 (1997) 195–232.
[37] V.A. Sheremet, G.R. Ierley, V.M. Kamenkovitch, Eigenanalysis of the two-dimensional wind-driven ocean circulation problem, J. Mar. Res. 55 (1997) 57–92.
[38] J. Pedlosky, Ocean Circulation Theory, Springer, New York, 1996.
[39] E. Simonnet, H.A. Dijkstra, Spontaneous generation of low-frequency modes of variability in the wind-driven ocean circulation, J. Phys. Oceanogr. 32 (2002) 1747–1762.
[40] E. Simonnet, R. Temam, S. Wang, M. Ghil, K. Ide, Successive bifurcations in a shallow-water ocean model, in: 16th Intl. Conf. Numerical Methods in Fluid Dynamics, in: Lecture Notes in Physics, vol. 515, Springer-Verlag, 1995, pp. 225–230.
[41] S.P. Meacham, Low-frequency variability in the wind-driven circulation, J. Phys. Oceanogr. 30 (2000) 269–293.
[42] K.I. Chang, K. Ide, M. Ghil, C.-C.A. Lai, Transition to aperiodic variability in a wind-driven double-gyre circulation model, J. Phys. Oceanogr. 31 (2001) 1260–1286.
[43] N.T. Nadiga, B.P. Luce, Global bifurcation of Shilnikov type in a double-gyre ocean model, J. Phys. Oceanogr. 31 (2001) 2669–2690.
[44] E. Simonnet, M. Ghil, K. Ide, R. Temam, S. Wang, Low-frequency variability in shallow-water models of the wind-driven ocean circulation. Part I: Steady-state solutions, J. Phys. Oceanogr. 33 (2003) 712–728.
[45] E. Simonnet, M. Ghil, K. Ide, R. Temam, S. Wang, Low-frequency variability in shallow-water models of the wind-driven ocean circulation. Part II: Time-dependent solutions, Oceanogr. 33 (2003) 729–752.
[46] E. Simonnet, M. Ghil, H.A. Dijkstra, Homoclinic bifurcations in the quasi-geostrophic double-gyre circulation, J. Mar. Res. 63 (2005) 931–956.
[47] P. Berloff, A. Hogg, W. Dewar, The turbulent oscillator: A mechanism of low-frequency variability of the wind-driven ocean gyres, J. Phys. Oceanogr. 37 (2007) 2363–2386.
[48] S. Kravtsov, P. Berloff, W.K. Dewar, M. Ghil, J.C. McWilliams, Dynamical origin of low-frequency variability in a highly nonlinear mid-latitude coupled model, J. Climate 19 (2007) 6391–6408.
[49] E. Simonnet, Quantization of the low-frequency variability of the double-gyre circulation, J. Phys. Oceanogr. 35 (2005) 2268–2290.
[50] F.W. Primeau, Multiple equilibria and low-frequency variability of the wind-driven ocean circulation, J. Phys. Oceanogr. 32 (2002) 2236–2256.
[51] E. Simonnet, On the unstable discrete spectrum of the linearized 2-D Euler equations in bounded domains, Physica D, sub judice.
[52] L. Sushama, M. Ghil, K. Ide, Spatio-temporal variability in a mid-latitude ocean basin subject to periodic wind forcing, Atmosphere-Ocean 45 (2007) 227–250. doi:10.3137/ao.450404.
[53] C.A. Katsman, H.A. Dijkstra, S.S. Drijfhout, The rectification of the wind-driven ocean circulation due to its instabilities, J. Mar. Res. 56 (1998) 559–587.
[54] R. Robert, J. Sommeria, Statistical equilibrium states for two-dimensional flows, J. Fluid. Mech. 229 (1991) 291–310.
[55] L.N. Trefethen, A. Trefethen, S.C. Reddy, T.A. Driscoll, Hydrodynamic stability without eigenvalues, Science 261 (1993) 578–584.
[56] F. Bouchet, J. Sommeria, Emergence of intense jets and Jupiter's great red spot as maximum entropy structures, J. Fluid. Mech. 464 (2002) 465–207.
[57] B.F. Farrel, P.J. Ioannou, Structural stability of turbulent jets, J. Atmos. Sci. 60 (2003) 2101–2118.
[58] H. Poincaré, Sur les équations de la dynamique et le problème des trois corps, Acta Math. 13 (1890) 1–270.
[59] A.A. Andronov, L.S. Pontryagin, Systèmes grossiers, Dokl. Akad. Nauk. SSSR 14 (5) (1937) 247–250.
[60] S. Smale, Differentiable dynamical systems, Bull. Amer. Math. Soc. 73 (1967) 199–206.
[61] A. Katok, B. Haselblatt, Introduction to the Modern Theroy of Dynamical Systems, in: Encycl. Math. Appl., vol. 54, Cambridge Univ. Press, 1995, p. 822.
[62] J. Robbin, A structural stability theorem, Ann. Math. 94 (1971) 447–449.
[63] C. Robinson, Structural stability of C^1 diffeomorphisms, J. Differential Equations 22 (1976) 28–73.

[64] R. Mañé, A proof of the C^1-stability conjecture, Publ. Math, I.H.E.S. 66 (1987) 161–210.
[65] J. Palis, A global perspective for non-conservative dynamics, Ann. I.H. Poincaré 22 (2005) 485–507.
[66] M. Peixoto, Structural stability on two-dimensional manifolds, Topology 1 (1962) 101–110.
[67] S. Smale, Structurally stable systems are not dense, Amer. J. Math. 88 (2) (1966) 491–496.
[68] S. Newhouse, The abundance of wild hyperbolic sets and nonsmooth stable sets for diffeomorphisms, Publ. Math. I.H.E.S. 50 (1979) 101–150.
[69] E.N. Lorenz, Deterministic nonperiodic flow, J. Atmos. Sci. 20 (1963) 130–141.
[70] J. Guckenheimer, R.F. Williams, Structural stability of Lorenz attractors, Publ. Math. I.H.E.S. 50 (1979) 59–72.
[71] R.F. Williams, The structure of Lorenz attractors, Publ. Math. I.H.E.S. 50 (1979) 73–99.
[72] Y. Sinai, Gibbs measures in ergodic theory, Russian Math. Surveys 27 (1972) 21–69.
[73] J.P. Eckmann, D. Ruelle, Ergodic theory of chaos and strange attractors, Rev. Modern Phys. 57 (1985) 617–656; Rev. Modern Phys. 57 (1985) 1115 (addendum).
[74] J.W.B. Lin, J.D. Neelin, Influence of a stochastic moist convective parameterization on tropical climate variability, Geophys. Res. Lett. 27 (2000) 3691–3694.
[75] J.W.B. Lin, J.D. Neelin, Considerations for stochastic convective parameterization, J. Atmos. Sci. 59 (2002) 959–975.
[76] J.W.B. Lin, J.D. Neelin, Toward stochastic deep convective parameterization in general circulation models, Geophys. Res. Lett. 30 (2003) 1162. doi:10.1029/2002GL016203.
[77] T.N. Palmer, The prediction of uncertainty in weather and climate forecasting, Rep. Prog. Phys. 63 (2000) 71–116.
[78] T. Jung, T.N. Palmer, G.J. Shutts, Geophys. Res. Lett. 32 (2005) Art. No. L23811.
[79] B. Stevens, Y. Zhang, M. Ghil, Stochastic effects in the representation of stratocumulus-topped mixed layers, in: Proc. ECMWF Workshop on Representation of Sub-Grid Processes Using Stochastic-Dynamic Models, 6–8 June 2005, Shinfield Park, Reading, UK, pp. 79–90.
[80] J.A. Langa, J.C. Robinson, A. Suarez, Stability, instability, and bifurcation phenomena in non-autonomous differential equations, Nonlinearity 15 (2002) 887–903.
[81] G. Sell, Non-autonomous differential equations and dynamical systems, Trans. Amer. Math. Soc. 127 (1967) 241–283.
[82] A. Berger, S. Siegmund, On the gap between random dynamical systems and continuous skew products, J. Dyn. Diff. Eq. 15 (2003) 237–279.
[83] J.F.B. Mitchell, Can we believe predictions of climate change? Quart. J. Roy. Meteorol. Soc. (Part A) 130 (2004) 2341–2360.
[84] I.M. Held, The gap between simulation and understanding in climate modeling, Bull. Amer. Meteo. Soc. 86 (2005) 1609–1614.
[85] J.C. McWilliams, Irreducible imprecision in atmospheric and oceanic simulations, PNAS 104 (21) (2007) 8709–8713.
[86] V.S. Anishchenko, T.E. Vadivasova, A.S. Kopeikin, J. Kurths, G.I. Strelkova, Effect of noise on the relaxation to an invariant probability measure of nonhyperbolic chaotic attractors, Phys. Rev. Lett. 87 (5) (2001) 054101-1–054101-4.
[87] V.S. Anishchenko, T.E. Vadivasova, A.S. Kopeikin, G.I. Strelkova, J. Kurths, Influence of noise on statistical properties of nonhyperbolic attractors, Phys. Rev. E 62 (2000) 7886.
[88] V.S. Anishchenko, T.E. Vadivasova, A.S. Kopeikin, G.I. Strelkova, J. Kurths, Peculiarities of the relaxation to an invariant probability measure of nonhyperbolic chaotic attractors in the presence of noise, Phys. Rev. E 65 (3) (2002) 036206.
[89] C. Grebogi, H. Kantz, A. Prasad, Y.C. Lai, E. Sinde, Unexpected robustness-against-noise of a class of nonhyperbolic chaotic attractors, Phys. Rev. E 65 (2002) 026209-1–026209-18.
[90] M.J. Feigenbaum, L.P. Kadanoff, S.J. Shenker, Quasiperiodicity in dissipative systems: A renormalization group analysis, Physica D 5 (1982) 370–386.
[91] P. Bak, R. Bruinsma, One-dimensional Ising model and the complete devil's staircase, Phys. Rev. Lett. 49 (1982) 249–251.
[92] P. Bak, The devil's staircase, Phys. Today 39 (12) (1986) 38–45.
[93] F.-F. Jin, J.D. Neelin, M. Ghil, El Niño on the Devil's Staircase: Annual subharmonic steps to chaos, Science 264 (1994) 70–72.
[94] F.-F. Jin, J.D. Neelin, M. Ghil, El Niño/Southern Oscillation and the annual cycle: Subharmonic frequency locking and aperiodicity, Physica D 98 (1996) 442–465.
[95] E. Tziperman, L. Stone, M. Cane, H. Jarosh, El Niño chaos: Overlapping of resonances between the seasonal cycle and the Pacific ocean-atmosphere oscillator, Science 264 (1994) 72–74.
[96] E. Tziperman, M.A. Cane, S.E. Zebiak, Irregularity and locking to the seasonal cycle in an ENSO prediction model as explained by the quasi-periodicity route to chaos, J. Atmos. Sci. 50 (1995) 293–306.
[97] P. Chang, L. Ji, H. Li, M. Flugel, Chaotic dynamics versus stochastic processes in El Niño-Southern Oscillation in coupled ocean-atmosphere models, Physica D 98 (1996) 301–320.
[98] A. Saunders, M. Ghil, A Boolean delay equation model of ENSO variability, Physica D 160 (2001) 54–78.
[99] M. Ghil, I. Zaliapin, S. Thompson, A delay differential model of ENSO variability: Parametric instability and the distribution of extremes, Nonlin. Proc. Geophys. 15 (2008) 1–17.
[100] Yu.A. Kuznetsov, Elements of Applied Bifurcation Theory, 3rd ed., Springer-Verlag, New York, 2004, p. 631.
[101] A. Denjoy, Sur les courbes définies par les équations différentielles à la surface du tore, J. Math. Pure Appl. 11 (IV) (1932) 333–375.
[102] T. Kaijser, On stochastic perturbations of iterations of circle maps, Physica D 68 (1993) 201–231.
[103] P.E. Kloeden, E. Platen, Numerical Solution of Stochastic Differential Equations, Springer, Berlin, 1992, p. 632.
[104] T. Caraballo, J.A. Langa, J.C. Robinson, A stochastic pitchfork bifurcation in a reaction-diffusion equation, Proc. R. Soc. Lond. A 457 (2001) 2041–2061.
[105] J. Duan, K. Lu, B. Schmalfuss, Smooth stable and unstable manifolds for stochastic evolutionary equations, J. Dyn. Diff. Eq. 16 (2004) 949–972.
[106] J. Duan, K. Lu, B. Schmalfuss, Invariant manifolds for stochastic partial differential equations, Ann. Probab. 31 (2003) 2109–2135.
[107] L. Arnold, K. Xu, Normal forms for random differential equations, J. Differential Equations 116 (1995) 484–503.
[108] L. Arnold, P. Imkeller, Normal forms for stochastic differential equations, Probab. Theory Related Fields 110 (4) (1998) 559–588.
[109] W. Li, K. Lu, Sternberg theorems for random dynamical systems, Comm. Pure Appl. Math. 58 (2005) 941–988.
[110] N.D. Cong, Topological Dynamics of Random Dynamical Systems, in: Oxford Mathematical Monographs, Clarendon Press, Oxford, 1997, p. 212.
[111] H. Crauel, F. Flandoli, Attractors for random dynamical systems, Scuola Normale Superiore Pisa 148 (1992), Technical Report.
[112] H. Crauel, A uniformly exponential attractor which is not a pullback attractor, Arch. Math. 78 (2002) 329–336.
[113] H. Zmarrou, A.J. Homburg, Bifurcations of stationary measures of random diffeomorphisms, Ergodic Theory Dynam. Systems 27 (2007) 1651–1692.
[114] S. Kuksin, A. Shirikyan, On random attractors for mixing-type systems, Funct. Anal. Appl. 38 (1) (2004) 34–46.
[115] V.I. Oseledets, A multiplicative ergodic theorem. Lyapunov characteristic numbers for dynamical systems, Trans. Moscow Math. Soc. 19 (1968) 197–231.
[116] L. Arnold, Trends and open problems in the theory of random dynamical systems, in: L. Accardi, C.C. Heyde (Eds.), Probability Towards 2000, in: Springer Lecture Notes in Statistics, vol. 128, 1998, pp. 34–46.
[117] N.D. Cong, Topological classification of linear hyperbolic cocycles, J. Dyn. Diff. Eq. 8 (1996) 427–467.
[118] T. Wanner, Linearization of random dynamical systems, in: C.K.R.T. Jonesm, U. Kirchgraber, H.O. Walther (Eds.), Dynamics Reported, vol. 4, Springer, Berlin, Heidelberg, New York, 1995, pp. 203–269.
[119] E.A. Coayla-Teran, P.R.C. Ruffino, Random versions of Hartman-Grobman theorems, Preprint IMECC, UNICAMP, No. 27/01, 2001.
[120] E.A. Coayla-Teran, S.A. Mohammed, P.R.C. Ruffino, Hartman-Grobman theorems along hyperbolic stationary trajectories, Discrete Contin. Dyn. Syst. A 17 (2) (2007) 281–292.